Compositions of trioctahedral micas in the Cornubian batholith

M. STONE[1], C. S. EXLEY[2], AND M. C. GEORGE[1]

[1]Department of Geology, The University, Exeter EX4 4QE
[2]Department of Geology, The University, Keele, Staffs ST5 5BG

Abstract

New major and trace element chemical analyses of trioctahedral micas of the Cornubian batholith emphasize their enrichment in a 'trace-alkali element' association (Li, Rb, Cs, F, Nb, Mn) and their deficiency in a 'femic element' association (Zr, Ce, Th as well as Mg and Ti) compared with micas from many other granite suites, although there are similarities with some Hercynian granites and with rare metal pegmatites. The new data demonstrate a continuous series from siderophyllite through zinnwaldite to lepidolite, principally as a result of Li–R^{2+} substitution as indicated by Foster (1960), although a more complete replacement is (Li, Al) = (Fe^{2+}, Fe^{3+}, Ti). It is suggested that the ranges of these micas are based upon the Li content in the unit cell formula and the ratio of Li to R^{2+}, in effect, a compromise between the ranges proposed by Foster (1960) and Rieder (1970). Microprobe analyses lack Li_2O, but can be plotted on FeO–SiO_2 and FeO–Al_2O_3–SiO_2 diagrams (wt. or atom %) in order to locate compositions within the trioctahedral Li–Fe micas and to distinguish between lepidolite and muscovite.

An examination of 55 new mica analyses shows that hornfels biotites are richer in Mg and that the Cornubian Type A granite (as classifed by Exley and Stone, 1982) micas are richer in Ti and Fe compared with those of Type B granites. Micas from microgranite dykes appear to be poorer in femic elements and richer in trace alkalis and F compared with their Type B granite hosts, consistent with their differentiation from the latter. Mica chemistry is consistent with the magmatic evolution of the A–B-microgranite sequence in the biotite granites, the transformation of Types B to D upon emplacement of E, the derivation of Types E from B by extreme differentiation or metasomatic transformation and mobilization, and the *in situ* differentiation of Types G from E.

KEYWORDS: micas, Cornubian batholith, granite, Cornwall.

Introduction

THE granites of the Cornubian batholith fall into two petrographic groups, namely, biotite granites and lithium-mica granites. They can be subdivided further into several types (Exley and Stone. 1982) as shown in Table 1. Of these, the Type B granites predominate, forming over 90% of the overall outcrop (Hawkes and Dangerfield, 1978) and other types are relatively minor. However, lithium micas occur in the Type E granites, which occupy a large proportion of the total outcrop in the Tregonning–Godolphin and St. Austell plutons, and in the Type D granite, apparently transitional between Types B and E, in the St. Austell pluton only (Fig. 1). Preliminary microprobe work (reported in Stone, 1984, and unpublished data) indicated that Types D and E granites contained zinnwaldite, whilst extreme differentiates, such as the leucogranites (Type G) at the roof of the Tregonning granite, contained lepidolite. Identification of these micas was based upon a comparision of their SiO_2, Al_2O_3 and F contents with those of fully analysed micas. The occurrence and composition of these Li micas is further substantiated by the work reported herein and by the recent work of Martin (1983). The important role played by the micas in the development and evolution of these granites is evident in their classification, in the petrology of the St. Austell (Exley, 1959; Manning and Exley, 1984) and Tregonning–Godolphin (Stone, 1975) granites and in a study of their textures (Stone, 1984).

Little previous work has been done on the micas of the Cornubian batholith as a whole. Exley and Stone (1964) summarize most of the available data on the micas up to 1964. Since then, biotites and

Mineralogical Magazine, April 1988, Vol. 52, pp. 175–192

Table 1. Granite types in the Cornubian batholith

Type	Name	Grain size	Minerals	Li-Fe mica	Occurrence
A	Basic micro-granite	fine	Pl>Or, (Hbl)	Bi	Inclusions in B
B	Biotite granite	coarse	Or>Pl,T,A, Cd,Mu	Bi	Main rock type, commonly megacrystic: includes all coarse biotite granites of Dangerfield et al.(1979)
C	Biotite granite	fine/ medium	Or>Pl,T,Mu	Bi	Dykes cutting B; rafts, rounded inclusions in B. Various sources.
D	Megacryst-ic Li-mica granite	coarse	Or=Pl($An_{<}$), T,Tp,Mu	Zinn	Modified B and transitional into B: occurs only in St. Austell pluton.
E	Aphyric Li-mica granite	medium	Pl(An_{0-4})>Or, T,Tp,Mu	Zinn	Emplaced into B/D at St. Austell; cuts C in Tregonning-Godolphin pluton.
F	Fluorite granite	medium	Fl,Mu	none	Alteration product of E (Manning and Exley, 1984).
'G'	Aphyric Li-mica leucogranite	medium	Pl(An_{0})>>Or, T,Tp	Lepid	Roof differentiates above E in Tregonning-Godolphin and St. Austell plutons.

A = andalusite, An = anorthite, Bi = biotite, Cd = cordierite (pinite), F = fluorite, Hbl = hornblende, Lepid = lepidolite, Mu = muscovite, Or = K-feldspar, Pl = Plagioclase feldspar, T = Tourmaline, Tp = topaz, Z = zinnwaldite.

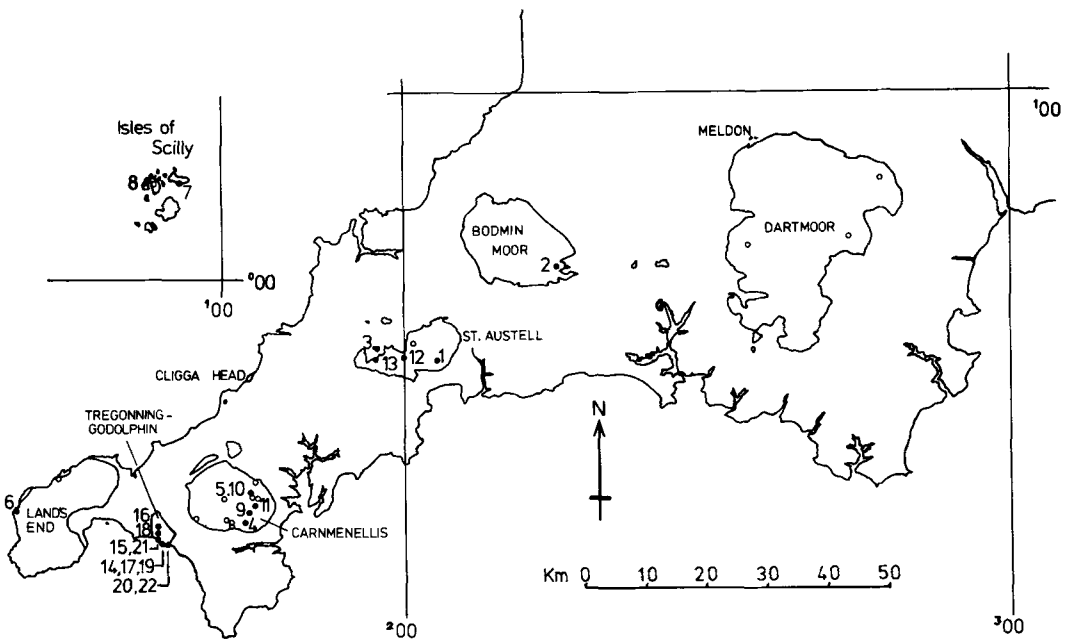

FIG. 1. Sketch map of S.W. England showing sample localities in the plutons of the Cornubian batholith. Solid circles, 22 chemically analysed micas; open circles, other mica analyses in the literature and new microprobe analyses.

their host rocks have been analysed from the Cligga (Hall, 1971) and Dartmoor (Al-Saleh *et al.*, 1977) plutons. An excellent account of lepidolites in the Meldon microgranite, together with many analyses, is given by Chaudhry and Howie (1973*a*). Recently, Martin (1983) has confirmed the occurrence of zinnwaldite, formerly identified by Exley (1959) and Cundy *et al.* (1960), in the St. Austell pluton.

This paper supplements existing data with more than 20 new full chemical analyses together with over 60 partial (microprobe) analyses of trioctahedral micas from the Cornubian batholith, confirms the occurrence of zinnwaldite in the Types D and E granites and of lepidolite in the roof differentiates of Type E and discusses the distribution of these micas. Sample localities for the new data and some previous data are shown in Fig. 1.

Methods

Altogether, 22 trioctahedral micas were fully analysed for all major and 20 trace elements, including Cs and Sn. Initial separation of the −60 mesh fractions with a Cook magnetic separator, and subsequent cleaning by the repeated use of heavy liquids yielded samples with over 98% purity. Major elements, except FeO, Li_2O and F, were determined by XRF spectrometry on fused beads (Harvey *et al.*, 1973). Trace elements were determined on powder discs bound with PVP, backed with boric acid and pressed at 3t for 3 minutes (Norrish and Hutton, 1964).

FeO was determined titrimetrically using ceric sulphate solution (BDH Convol—0.05 N) and N-phenylanthranilic acid in sodium carbonate solution as a redox indicator (French and Adams, 1972) after dissolution of the sample by HF–H_2SO_4 attack in a sealed, thick-walled, polypropylene bottle. For Li_2O, a separate portion of each sample was digested in an HF-aqua regia mixture in a pressure bomb, and subsequently analysed by atomic emission spectrophotometry using a high-temperature nitrous-oxide–acetylene flame in a Pye Unicam SP1900. Fluorine was determined with a Pye Unican PW9416 selective ion analyser after fusion of another portion of each sample with alkali carbonate in a platinum crucible, dissolution, the addition of TISAB buffer solution and making up to volume following a procedure modified after Troll *et al.* (1977).

These data are supplemented by over 60 average partial analyses of micas determined by electron microprobe on highly polished uncovered thin sections coated with a 20 nm thick carbon film. Analyses were performed using a C.A.-M.E.C.A. Camebax microprobe (combined EDS and WDS) in the Geology Department of the University of Manchester. These micas were analysed for F, Rb and Cs and, in some instances, Sn, in addition to the usual major elements. Of course, Li is missing from these analyses so that formulae cannot be calculated directly and the proportions of Fe^{3+} and Fe^{2+} cannot be estimated accurately.

Data were processed on a Prime 750 computer with the help of the Minitab package and Fortran programs written or modified by one of us (MS). Coefficients of variation and the Kolmogorov–Smirnov (K–S) statistics indicate that the major elements have near normal distributions and that parametric statistical procedures are applicable. Of the trace elements that have high coefficients of variation (>1.0) and high K–S statistics (As, Ba, Cr, Pb and Sr), only Sr has a K–S value that leads to the rejection of the null hypothesis for a normal distribution at the 0.001 confidence level.

Chemistry and chemical variation

Table 2 gives major and trace element contents of 22 newly analysed micas (11 biotites, 7 zinnwaldites and 4 lepidolites) from various parts of the Cornubian batholith (Fig. 1). In both this table and Table 4, the type of granite host is indicated by the letters B, D and E (Exley and Stone, 1982, and Table 1 in this paper) and G for the leucogranites in the roof complex of the Tregonning granite. The principal features of these Cornubian micas are their high contents of trace alkali elements (Li, Rb and Cs), F, Nb, and Sn, and low contents of Ba, Zr, and Sr, which reflect the geochemistry of their host rocks. Even the biotites show these characteristics, together with low MgO and TiO_2, when compared with those from many other granites, for example, Caledonian granite complexes in Scotland (Deer, 1937; Nockolds and Mitchell, 1948; Haslam, 1968) and calc-alkaline suites from elsewhere, such as the Sierra Nevada batholith (Dodge *et al.*, 1969) and the Murrumbidgee batholith, S.E. Australia (Joyce, 1973). However, some comparison can be made with biotites from the later members of the stanniferous Devonian Halifax pluton of Nova Scotia (Smith *et al.*, 1982) and Mole granite of New South Wales (Plimer and Kleeman, 1986) and with the Hercynian granites of northern Portugal (Neiva, 1976), also stanniferous, and Brittany (Barriere and Cotten, 1979). There are also very close similarities with the Li-micas from the Hercynian granites of the Krušné Hory Mountains in northern Czechoslovakia (Rieder, 1970) and

TABLE 2. Major and trace element analyses of Li-Fe micas

	1	2	3	4	5	6	7	8	9	10	11	12	13	14	15	16	17	18	19	20	21	22
Type	B	B	B	B	B	B	B	B	B	B	B	D	E	E	E	E	E	E	G	G	G	G
Sample	E179	EB52	E259	0020	0021	0359	0465	0467	0620	0630	0631	E249	E250	0002	0004	0007	0045	0088	0034	0042	0083	0084
(weight %)																						
SiO_2	37.27	36.03	37.35	36.45	37.34	35.22	35.30	34.63	39.96	35.19	34.77	42.97	48.48	41.79	49.73	49.01	44.81	48.17	51.83	52.55	52.84	51.81
TiO_2	2.18	2.31	0.38	2.73	2.52	2.57	2.64	2.99	2.68	2.40	2.76	0.84	0.34	1.40	0.35	0.36	0.44	0.45	0.21	0.20	0.20	0.26
Al_2O_3	22.70	21.62	22.08	21.61	20.81	21.67	21.84	22.95	21.99	21.94	22.30	22.87	20.06	22.60	20.93	20.79	22.43	23.16	19.11	20.55	19.57	19.72
Fe_2O_3	2.96	3.92	1.30	3.44	2.99	2.58	3.22	3.35	2.60	1.72	1.98	2.28	1.19	1.45	0.79	1.00	0.19	1.12	0.25	n.d	0.45	0.44
FeO	16.91	20.67	19.84	18.08	18.35	21.57	18.29	18.31	18.95	19.39	19.21	10.49	9.89	15.57	8.61	9.11	11.08	8.58	3.75	3.22	2.96	4.56
MnO	0.65	0.55	0.37	0.40	0.39	0.27	0.37	0.29	0.38	0.46	0.36	0.48	0.13	0.64	0.44	0.51	0.43	0.40	1.10	1.11	1.33	1.22
MgO	2.59	3.64	0.68	4.49	4.51	1.91	3.94	4.52	3.82	3.54	3.94	0.96	0.12	0.75	n.d.	0.03	0.39	0.08	0.23	0.24	n.d.	0.24
CaO	0.33	0.36	0.09	0.31	0.28	0.11	0.17	0.21	0.18	0.46	0.72	0.13	0.16	0.14	0.35	0.14	0.12	0.16	0.23	0.26	0.24	0.21
Na_2O	0.70	0.74	n.d.	0.68	0.54	n.d.	n.d.	n.d.	1.02	n.d.	n.d.	2.06	0.69	0.83	0.76	0.68	n.d.	0.77	n.d.	0.31	0.57	n.d.
K_2O	8.41	8.27	9.02	8.19	8.68	8.68	8.46	8.12	9.07	8.26	7.71	9.24	9.66	9.10	9.40	9.54	9.55	9.40	9.15	9.12	9.29	9.63
Li_2O	1.30	1.01	1.59	0.90	0.89	0.74	0.58	0.57	0.98	0.93	0.76	2.94	3.97	2.61	3.83	4.02	2.84	2.78	4.65	4.43	5.81	4.89
F	2.87	1.65	4.53	1.59	1.73	2.57	1.14	0.77	2.20	2.66	1.99	5.75	6.30	5.07	4.75	7.31	6.46	4.79	7.41	7.01	6.17	7.28
(ppm)																						
As	18	8	2	2	2	83	24	5	5	6	6	1	1	30	2	1	2	13	1	1	1	6
Ba	163	169	n.d	297	241	87	355	592	305	160	270	n.d	n.d	n.d	n.d	n.d	n.d	n.d	n.d	n.d	n.d	n.d
Ce	260	93	47	122	114	92	256	203	175	246	65	87	58	148	141	120	60	58	105	45	91	139
Cr	91	116	12	190	198	15	99	57	188	158	169	10	5	247	n.d	n.d	3	n.d	n.d	n.d	n.d	n.d
Cs	694	220	252	386	399	292	287	85	344	456	339	676	646	806	1363	1401	525	623	1518	921	1611	1787
Cu	6	3	n.d	14	10	8	6	n.d	n.d	3	n.d	14	9	3	n.d	4	n.d	52	n.d	9	2	n.d
Ga	66	58	105	60	64	77	61	73	83	70	64	85	77	92	94	97	99	103	80	81	81	86
La	171	55	53	70	60	48	133	86	92	130	144	104	111	128	157	165	80	74	219	130	182	261
Nb	216	120	365	117	113	272	106	179	121	172	99	172	148	234	193	213	224	190	161	124	159	201
Ni	53	81	49	70	90	71	70	39	107	78	98	54	96	101	88	95	71	63	103	101	143	106
Pb	12	15	n.d	6	5	26	15	21	12	14	6	n.d	n.d	n.d	n.d	n.d	n.d	n.d	n.d	n.d	n.d	n.d
Rb	2783	1761	4396	1736	1872	2377	1495	1205	2129	2021	1815	5298	8089	5398	6852	7275	6356	6262	8426	8492	8949	8744
Sn	76	27	9	30	34	24	32	44	33	53	31	61	19	79	73	73	60	99	78	70	74	69
Sr	4	2	1	5	2	2	2	4	n.d	2	2	1	7	3	37	6	5	5	60	14	24	5
Th	54	19	7	-	-	23	67	62	-	38	39	16	13	--	--	--	10	--	14	14	15	7
U	26	24	9	-	-	134	18	18	-	26	14	12	24	--	--	--	12	--	20	29	19	26
V	203	182	18	211	190	125	182	210	216	219	219	52	58	150	42	42	27	23	53	33	50	60
Y	90	27	33	n.d	n.d	109	33	35	n.d	51	31	60	85	n.d	n.d	n.d	49	n.d	97	93	1	59
Zn	387	704	525	484	608	305	573	495	558	497	443	234	59	544	559	621	375	355	319	306	335	402
Zr	265	98	1	53	66	76	316	234	127	182	197	53	8	161	17	13	3	15	21	19	21	17

Rock types as in Table I.
Sample refers to sample numbers: see Appendix.
n.d. not detected; -- not determined.

Table 3. Selected Pearson product moment correlation coefficients

	SiO_2	TiO_2	Al_2O_3	FeO	MnO	MgO	K_2O	Li_2O	F
TiO_2	-0.902								
Al_2O_3	-0.594	0.420							
FeO	-0.975	0.847	0.548						
MnO	0.645	-0.489	-0.578	-0.706					
MgO	-0.842	0.948	0.255	0.763	-0.406				
K_2O	0.811	-0.860	-0.353	-0.726	0.298	-0.853			
Li_2O	0.976	-0.898	-0.622	-0.956	0.704	-0.863	0.786		
F	0.902	-0.940	-0.458	-0.865	0.562	-0.937	0.844	0.916	
Ba	-0.308	0.788	0.444	-0.439	-0.425	0.695	-0.211	-0.579	-0.819
Ce	-0.422	0.534	0.185	0.351	-0.078	0.516	-0.395	-0.400	-0.478
Cs	0.863	-0.721	-0.662	-0.853	0.763	-0.660	0.634	0.895	0.780
La	0.586	-0.415	-0.543	-0.642	0.709	-0.337	0.291	0.640	0.532
Nb	0.034	-0.352	0.179	0.058	-0.069	-0.500	0.322	0.080	0.287
Ni	0.546	-0.320	-0.724	-0.506	0.599	-0.206	0.336	0.598	0.421
Rb	0.975	-0.949	-0.566	-0.937	0.619	-0.921	0.845	0.979	0.959
Sn	0.646	-0.511	-0.051	-0.687	0.557	-0.505	0.437	0.595	0.553
Sr	0.588	-0.460	-0.603	-0.599	0.495	-0.317	0.299	0.575	0.437
Th	-0.617	0.800	0.418	0.495	-0.319	0.818	-0.707	-0.635	-0.771
Y	0.262	-0.244	-0.155	-0.220	0.045	-0.622	0.325	0.191	0.382
Zr	-0.738	0.740	0.472	0.660	-0.295	0.645	-0.721	-0.694	-0.706

	Ba	Ce	Cs	La	Nb	Rb	Sn	Sr	Th
Ce	0.231								
Cs	-0.572	-0.112							
La	0.027	0.244	0.837						
Nb	-0.329	-0.142	0.058	-0.102					
Rb	-0.767	-0.471	0.834	0.568	0.186				
Sn	-0.044	0.068	0.666	0.553	0.042	0.574			
Sr	0.408	-0.098	0.624	0.511	-0.089	0.528	0.407		
Th	0.711	0.837	-0.414	0.038	-0.306	-0.702	-0.042	-0.279	
Y	-0.519	-0.042	0.172	0.177	0.227	0.296	0.244	0.255	-0.152
Zr	0.377	0.774	-0.538	-0.061	-0.166	-0.718	-0.269	-0.363	0.873

the Erzgebirge of the G.D.R. (Palchen and Tischendorf, 1974) and from many rare metal pegmatites of widely different ages.

Correlation coefficients for most of the raw data of Table 2 are shown in Table 3. Associations are indicated by high positive coefficients whilst substitutions and closed sum effects are indicated by negative coefficients. In general, of the oxides not indicated in Table 3, Fe_2O_3 follows FeO; CaO and Na_2O have few associations. Amongst the trace elements, U shows little association except for a significant positive correlation with Pb. Note that Ba is undetected in most of the Li micas, therefore has a stronger concentration in biotite and hence a strong association with the femic elements.

Two clearly opposed associations emerge from a perusal of the data: these are a 'fluoride–alkali' association (K_2O, Li_2O, Rb, Cs, F, Mn, La, Ga) and a 'femic' association (TiO_2, Fe_2O_3, FeO, MgO, Zr, V, Th, Ce). R-mode cluster analysis confirms this pattern and shows in addition a mixed, largely unrelated group of elements, some of which occur in included accessory minerals in the micas (Ce, Y, La). Ce is strongly correlated with Th and Zr (also in included minerals), Y with U, and La with the trace alkalis and fluorine. To a large degree, as might be expected, these associations reflect the element associations found in the differentiation sequence from biotite granite to late-stage Li-rich leucogranite (Stone, 1975, 1982). Indeed, the trioctahedral mica compositions clearly dominate much of the element variation in these rocks.

The first two groupings are illustrated by the plots in Fig. 2. Such bivariate plots yield lines with positive slopes for strongly associated elements within groups (or clusters) and negative slopes for comparisons of elements between groups. Typical of the former is the Li_2O–SiO_2 diagram (Fig. 2*a*; reflected also in the formula Li–Si plot) in which about 95% of the Li variation is accounted for by the regression equation

$$Li_2O = 0.236\,SiO_2 - 7.56$$

Fig. 2*a*, like many using the data presented in this paper and Q-mode cluster analysis, clearly categorizes the three groups of trioctahedral micas considered here. This is believed to reflect the sampling of clear-cut rock types since evidence presented below indicates that there is a continuous series within the Li-Fe micas.

Sn is associated with the 'fluoride–alkali' element group, though somewhat less strongly, as illustrated in the Sn–SiO_2 plot of Fig. 2*b*. Similar

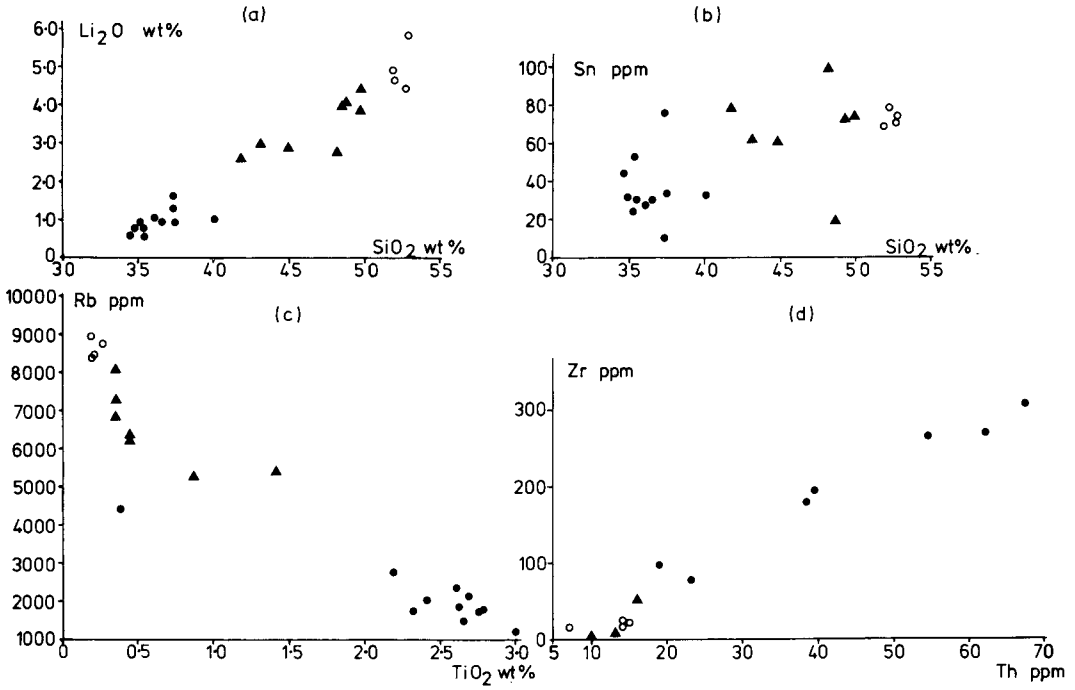

FIG. 2. Variation diagram of raw data. (*a*) Li_2O–SiO_2 (wt. %); (*b*) Sn (ppm)–SiO_2 (wt. %); (*c*) Rb (ppm)–TiO_2 (wt. %); (*d*) Zr–Th (ppm). Solid circles, biotites; triangles, zinnwaldites; open circles, lepidolites.

relationships occur in the host rocks (Stone, 1982). Sn occurs in cassiterite inclusions and some may be present in the mica structure (Štemprok and Šulcek, 1969; Neiva, 1976). Probe analyses on several points within a mica show a scatter in Sn values, partly the result of working near the lower limit of detection, but perhaps also reflecting inhomogeneity of Sn within the micas and possibly indicating the presence of submicroscopic cassiterite grains. The correlation between Sn and Li and also between Sn and Si (or SiO_2) (Table 3 and Neiva, 1976) does not necessarily imply that Sn is held in the mica structure. Despite the correlation between Sn and Li from biotites in Hercynian granites in northern Portugal, Neiva (1976) states that 'The biotites contain less than 21% of the tin content of the granites ...', so that only a fifth of the tin at most could occur within the structure, yet Li, with which it is correlated, is almost completely held in the mica structures. A similar type of relationship occurs between Zr and the femic elements (Fe and Mg), as discussed below.

An example of the comparison of elements between the fluoride–alkali and femic groups is given in the Rb–TiO_2 plot of Fig. 2*c*. Again, there is a clear separation of the main mica groups, although a low Ti biotite with high Rb plots close to the Li micas and the separation within the latter group is not marked.

The close Zr–'femic' element association (like Th, V and often Ce) might suggest a structure relationship between Zr and the femic elements. However, the small size and high charge of Zr make it an unlikely candidate. The principal accessory minerals in these granites have been identified by Jefferies (1984, 1985) and Charoy (1986) as zircon, monazite, xenotime, uraninite, apatite and ilmenite, all of which may be included in mica, sometimes on a microscopic scale which precludes effective separation. These authors have shown that the rare earth elements occur largely in the first three minerals named. La and Ce along with Th occur mostly in monazite, whilst xenotime and zircon account for the heavy rare earths (Jefferies, 1985) and the latter mineral contains most and perhaps all of the Zr in the rock. Of course, U occurs in uraninite. This distribution would account for the marked associations between most of these elements, as shown e.g. in the Zr–Th plot (Fig. 2*d*), and make it unlikely that significant amounts are incorporated in the

mica structures themselves despite the strong positive correlations.

Formulae and formula variation

Formulae of the fully analysed trioctahedral micas (Table 4) have been calculated on an anhydrous basis of 22 oxygen atoms, owing to the lack of determination of H_2O^+. The octahedral (Y) site always contains more than 5 atoms and usually has >5.5 atoms, thereby confirming the trioctahedral nature of all these micas. Deficiency in the X-site (i.e. where the number of atoms falls well below 2) may reflect post-magmatic leaching and/or substitution by H_3O^+ ions, as suggested by Chaudhry and Howie (1973*a*) for the Meldon lepidolites. A plot of the formula compositions on the octahedral cation Li–Al–Fe^{2+} diagram of Foster (1960) is given in Fig. 3. Included in the figure are other composition points from earlier analyses of trioctahedral micas from south-western granites and the field of data points of lepidolites from the Type G Meldon microgranite (Chaudhry and Howie, 1973*a*).

In her account of the lithium micas, Foster (1960) suggests that there is a complete composition series from siderophyllite, through the protolithionites and the zinnwaldites to lepidolite on the one hand and a partial series between muscovite and lepidolite, broken in the middle by mixed forms composed of lithian muscovite and aluminous lepidolite, on the other. Fig. 3 shows a spread in lepidolite compositions towards the region of mixed lepidolite–muscovite forms. This is particularly the case with the Meldon data. However, it is the continuity in composition between lepidolite and siderophyllite that is of principal interest here. Clearly, the apparent gaps between the lepidolite, zinnwaldite and biotite fields in the cornubian micas are illusory: the two zinnwaldite composition points (15 and 16) closest to the lepidolite composition field could have been included in a slightly extended lepidolite field and there is no real evidence for a break here. A wider gap between zinnwaldite and biotite is partly closed by specimen 0002 (Table 2, col. 14), from a contact granite rich in dark mica, tourmaline and xenolithic pelitic material from the roof complex of the Tregonning granite, and by the data points for several other samples, including E179 and E259 from the St. Austell pluton (Table 2, cols. 1 and 3 respectively) and the two 'protolithionites' from Cligga Head. Of course, gaps of this sort in variation diagrams can be real, but commonly reflect sampling or lack of good exposure at the present erosion level. In any case, such a gap appears to be completely bridged by the probe data shown in Figs. 6 and 7 and by the data of Table 5. Clearly Li has not been determined in these analyses, but the marked increase in F, Rb and Cs and decrease in Fe from hornfels to granite in Table 5 indicate a complete bridging of composition points between biotite and zinnwaldite. At such contacts, this is envisaged as arising by ion-exchange between (Mg,Fe) and (Li,Al), i.e. a conversion of metamorphic biotite in the hornfels to zinnwaldite as the contact with the zinnwaldite-bearing granite is approached over a scale of a few mm.

The formula data in Table 4 can also be plotted on a triangular diagram proposed by Rieder (1970). As in the Foster diagram, this utilizes the octahedral cations Li, Mg, "Fe" (i.e. Fe^{2+} + Mn^{2+}) and $R(\text{oct})^{3+}$ (i.e. Al + Fe^{3+}). These are used to construct three ratios, namely: $A = 2LR/(2LR + \text{"Fe"})$; $B = \text{"Fe"}/(\text{"Fe"} + \text{Mg})$ and $C = \text{Mg}/(\text{Mg} + 2LR)$, where LR = Li or $R(\text{oct})^{3+}$, whichever is smaller and "Fe" = Fe^{2+} + Mn. The last two parameters are also related by $Q = R(\text{exc})^{3+}/E(\text{oct})$, where $R(\text{exc})^{3+} = R(\text{oct})^{3+} - \text{Li}$ and $E(\text{oct})$ is the sum of octahedral cations. Data can now be plotted in the Li–Mg–Fe^{2+}–R^{3+} pyramid illustrated by Rieder (1970, Figs. 2 and 3). For details of the construction the reader is referred to the original paper. Fig. 4 is a plot on the front (Li–Fe^{2+}–R^{3+}) face of this pyramid: such a plot is justified by the generally low Mg contents of these micas and particularly those rich in Li, so that most of the points plot on or fairly close to this front face and can readily be projected on to it. The plots of the Li–Al–Fe micas from the Cornubian batholith in Fig. 4 are similar to those of the data points given by Rieder (1970) of micas mainly from the Krušné Hory Mountains in Czechoslovakia and East Germany. It shows that data points lie close to a line that extends from the composition point of ideal siderophyllite to a region between trilithionite and polylithionite, though closer to the former (clustering in the region of Q-values between 0 and −1). Again, a continuous series is suggested, although there is a marked gap between the biotites and the zinnwaldites as well as a possible gap between the latter and the lepidolites. That these distributions result from sampling and do not reflect immiscibility is indicated by the more nearly continuous data plotted by Rieder (1970, Fig. 5) who follows Foster (op. cit.) in suggesting that there is a complete composition series between the lepidolites and siderophyllite.

Formula variation is clearly shown in bivariate plots between elements or between elements and A' (where $A' = LR/(LR + \text{"Fe"})$). The Li–Si diagram (not shown, but similar to the Li_2O–SiO_2

Table 4. Formulae of Li-Fe micas on the basis of 22 oxygen atoms

	1	2	3	4	5	6	7	8	9	10	11	12	13	14	15	16	17	18	19	20	21	22
Type	B	B	B	B	B	B	B	B	B	B	B	D	E	E	E	E	E	E	G	G	G	G
Sample	E179	EB5/2	E259	0020	0021	0359	0465	0467	0620	0630	0631	E249	E250	0002	0004	0007	0045	0088	0034	0042	0083	0084
Si	5.504	5.290	5.750	5.369	5.503	5.368	5.333	5.182	5.397	5.365	5.279	6.032	6.745	5.964	6.788	6.748	6.463	6.641	7.207	7.165	7.112	7.075
Al	2.496	2.710	2.250	2.631	2.497	2.614	2.667	2.818	2.603	2.635	2.721	1.968	1.255	2.036	1.212	1.252	1.537	1.359	0.793	0.835	0.888	0.925
Z	8.000	8.000	8.000	8.000	8.000	8.000	8.000	8.000	8.000	8.000	8.000	8.000	8.000	8.000	8.000	8.000	8.000	8.000	8.000	8.000	8.000	8.000
Al	1.455	1.031	1.756	1.120	1.118	1.291	1.222	1.229	1.182	1.307	1.269	1.981	2.034	1.765	2.155	2.121	2.276	2.404	2.339	2.467	2.216	2.249
Ti_{3+}	0.242	0.255	0.044	0.302	0.279	0.296	0.338	0.336	0.294	0.275	0.315	0.089	0.036	0.150	0.036	0.037	0.048	0.047	0.022	0.020	0.020	0.053
Fe_{2+}	0.329	0.434	0.151	0.381	0.332	0.297	0.366	0.377	0.286	0.197	0.226	0.241	0.374	0.156	0.081	0.104	0.021	0.116	0.026	--	0.046	0.045
Fe	2.088	2.538	2.554	2.227	2.262	2.758	2.311	2.291	2.314	2.472	2.439	1.231	1.151	1.858	0.983	1.049	1.337	0.989	0.436	0.367	0.333	0.521
Mn	0.081	0.068	0.048	0.050	0.049	0.035	0.047	0.037	0.047	0.059	0.046	0.057	0.015	0.077	0.051	0.059	0.053	0.047	0.130	0.128	0.152	0.141
Mg	0.570	0.797	0.156	0.981	0.991	0.435	0.887	1.008	0.832	0.804	0.892	0.201	0.025	0.160	--	0.006	0.084	0.016	0.048	0.049	--	0.049
Li	0.770	0.598	0.986	0.535	0.529	0.453	0.352	0.344	0.576	0.567	0.465	1.660	1.715	1.495	2.104	2.223	1.648	1.540	2.599	2.431	3.146	2.683
Y	5.535	5.721	5.695	5.601	5.560	5.565	5.523	5.622	5.531	5.681	5.652	5.460	5.350	5.661	5.410	5.599	5.467	5.159	5.600	5.462	5.913	5.741
Ca	0.052	0.057	0.015	0.049	0.044	0.018	0.028	0.034	0.028	0.075	0.117	--	0.024	0.021	0.051	0.021	0.019	0.024	0.034	0.038	0.035	0.031
Na	0.200	0.211	--	0.194	0.154	--	--	--	0.289	--	--	0.561	0.186	0.230	0.201	0.181	--	0.206	--	0.082	0.149	--
K	1.584	1.549	1.772	1.539	1.632	1.693	1.630	1.550	1.690	1.606	1.493	1.655	1.715	1.657	1.637	1.676	1.757	1.653	1.623	1.586	1.595	1.678
Rb	0.029	0.018	0.048	0.018	0.019	0.026	0.016	0.013	0.022	0.022	0.019	0.052	0.079	0.054	0.066	0.070	0.064	0.061	0.082	0.081	0.085	0.084
Cs	0.005	0.001	0.002	0.003	0.003	0.002	0.002	0.001	0.002	0.003	0.002	0.004	0.004	0.005	0.008	0.009	0.003	0.004	0.010	0.006	0.010	0.011
Ba	--	0.001	--	0.002	0.002	0.001	0.002	0.004	0.002	0.002	0.002	--	--	--	--	--	--	--	--	--	--	--
X	1.870	1.837	1.837	1.805	1.854	1.740	1.678	1.602	2.033	1.708	1.633	2.272	2.008	1.967	1.963	1.957	1.843	1.948	1.749	1.793	1.874	1.804
F	1.341	0.766	2.206	0.741	0.806	1.241	0.545	0.364	1.016	1.282	0.956	2.553	2.772	2.288	2.050	3.183	2.947	2.088	3.259	3.023	2.626	3.144
Foster parameters (Fig. 3)																						
Li_{3+}	13.9	10.5	17.3	9.6	9.5	8.1	6.4	6.1	10.4	10.0	8.7	30.4	32.1	26.4	38.9	39.7	30.1	29.9	46.4	44.5	53.2	46.7
R_{3+}	36.3	30.1	34.3	32.2	31.1	33.9	34.9	34.5	31.9	31.3	28.0	42.3	45.7	36.6	42.0	40.4	42.9	49.8	42.6	45.5	38.6	40.9
R^{2+}	49.5	59.5	48.4	58.3	59.4	58.0	58.8	59.3	57.7	58.7	63.3	27.3	22.3	37.0	19.1	19.9	27.0	20.4	11.0	10.0	8.2	12.4
Rieder parameters (Fig. 4)																						
A	0.415	0.315	0.431	0.320	0.314	0.245	0.230	0.228	0.328	0.309	0.272	0.720	0.746	0.607	0.803	0.801	0.703	0.748	0.894	0.908	0.904	0.780
Q	0.227	0.196	0.343	0.226	0.216	0.257	0.285	0.284	0.214	0.213	0.320	0.119	0.136	0.102	0.031	0.007	0.127	0.199	-0.038	0.010	-0.146	-0.059
A'	0.262	0.187	0.275	0.186	0.190	0.140	0.130	0.129	0.196	0.183	0.158	0.563	0.592	0.436	0.670	0.667	0.542	0.598	0.808	0.831	0.825	0.780

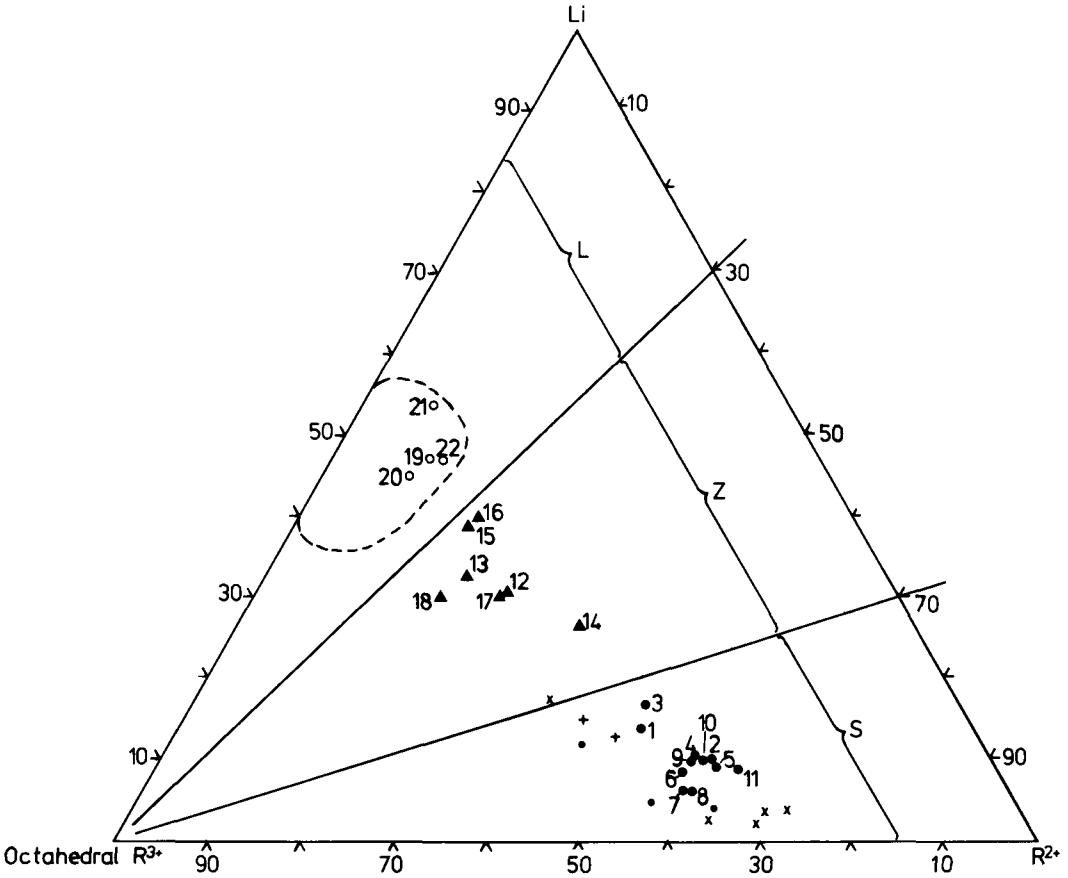

FIG. 3. Octahedral Li–R^{2+}–R^{3+} (incl. Ti) diagram (after Foster, 1960). New analyses—● biotite, ▲ zinnwaldite, ○ lepidolite: specimen numbers correspond with column numbers in Tables 2 and 4. Earlier biotite analyses: + Cligga (Hall, 1971); × Exley and Stone (1964); • Dartmoor (Al-Saleh *et al.*, 1977). Dashed line encloses the field defined by 16 lepidolite analyses from the Meldon microgranite (Chaudhry and Howie, 1973*a*). Boundaries between lepidolite and zinnwaldite at $Li_{70}R^{2+}_{30}$ and between the latter and siderophyllite at $LI_{30}R^{2+}_{70}$ indicated.

diagram of Fig. 2*a*) shows a clear linear relationship (with $r = +0.965$) in contrast to the wide scatter referred to and illustrated by Foster (1960, Fig. 36). This trend is consistent with increasing Si, decreasing tetrahedral Al, decreasing Fe^{2+} with increasing Li from siderophyllite to lepidolite. The Li–Fe^{2+} trend ($r = -0.954$) of Fig. 5*a* confirms this and is similar to Fig. 35 of Foster (1960), who suggests that the replacement ratio between Li and Fe^{2+} is between 2:1 and 1:1, at roughly 1.5:1. The regression equation for the data of Fig. 5*a* is

$$Li = 3.05 - 1.03Fe^{2+},$$

giving a ratio of nearly 1 : 1 (even when the dependent and independent variables are interchanged!), somewhat lower than that given by Foster although within the range stated by her. As that author points out, her triangular diagram (Foster, 1960, Fig. 37) indicates that octahedral trivalent (and tetravalent) elements are not involved in the replacement. However, Fig. 3 of the present paper indicates that Li enrichment is accompanied by a slight increase in octahedral R^{3+}; this is more clearly expressed by the close Li and octahedral Al (i.e. Al (6)) association ($r = +0.902$) related by the equation

$$Li = -1.40 + 1.58\,Al(6).$$

A glance at Table 4 shows that whilst octahedral occupancy changes little in the series, Al(6) increases from just over 1 to nearly 2.5 atoms per formula unit with increase in Li and decrease in Fe^{2+}.

Table 5. Biotite to zinnwaldite at a granite contact

	Traverse A					Traverse B				
	1	2	3	4	5	1	2	3	4	5
SiO_2	47.36	40.88	39.12	39.51	37.61	45.03	41.37	39.77	38.88	37.07
TiO_2	0.41	2.16	1.59	0.98	1.92	0.51	1.80	0.84	1.41	1.93
Al_2O_3	21.07	22.09	23.66	23.51	21.63	21.83	22.42	24.20	22.71	21.80
tFeO	9.98	16.36	17.33	17.21	20.61	11.30	14.09	16.51	17.83	22.30
MnO	0.54	0.46	0.59	0.66	0.46	0.68	0.54	0.65	0.46	0.42
MgO	0.29	0.57	0.57	1.14	2.04	0.43	0.56	1.02	1.44	1.96
Na_2O	0.40	0.32	0.41	0.43	n.d.	n.d.	0.58	0.43	0.35	n.d.
K_2O	10.11	9.56	9.65	9.74	9.29	10.22	9.74	9.70	9.55	9.44
Rb_2O	0.89	0.75	0.52	0.61	0.57	0.71	0.78	0.57	0.65	0.50
Cs_2O	0.14	0.16	0.05	0.04	0.06	0.21	0.12	0.03	0.08	0.05
F	7.68	5.83	4.91	6.76	3.67	6.94	5.83	5.24	4.55	2.94

Microprobe traverses over about 1.5 cm at intervals of c. 3 mm in contact hornfels, specimen 0516, Praa Sands.
tFeO is total iron as FeO.

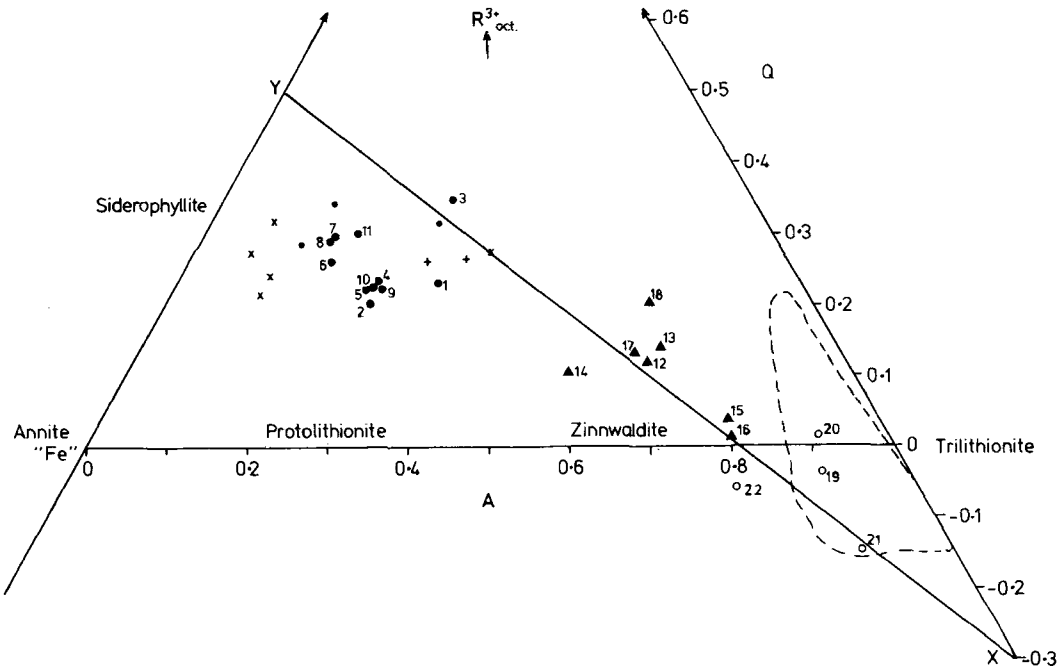

FIG. 4. Octahedral A–Q plot (after Rieder, 1970). $A = 2LR/(2LR + \text{"Fe"})$, where LR is Li or $(Al + Fe^{3+})$, whichever is smaller and "Fe" is $(Fe^{2+} + Mn^{2+})$; Q = octahedral $\{(Al + Fe^{3+}) - Li\}$/sum of octahedral cations. Other symbols as in Fig. 3.

Similar plots with A' (defined above and in caption of Fig. 5) as the abscissa show the continuity of variation of elements in the mica formulae (or wt. %) close to the 'join' X–Y (polylithionite to near siderophyllite), in Fig. 4. This is illustrated by the Rb–A' diagram Fig. 5*b*, which is almost identical with the F–A' plot (not shown). Both Rb and F show high positive correlation with A',

i.e. with increasing 'lepidolite' component in the series from siderophyllite to lepidolite.

Nomenclature

We are now able to consider critically the classification and nomenclature of the Cornubian Li–Fe micas.

A solid-solution series proposed by Rieder (1970) to cover the range of Li–Fe micas has the general formula:

$$K_2Fe_x^{2+}Li_{4-x}(Al,Fe^{3+})_2(Al_xSi_{8-x}O_{20})(OH,F)_4$$

with boundaries drawn as follows: siderophyllite, $x = 3 - 4$; zinnwaldite, $1 < x < 3$; and polylithionite, $x < 1$. However, the Rieder formula assumes full occupancy of the octahedral sites, which is uncommonly the case. It also assumes that the principal variables in these sites are Li and Fe^{2+}, with constant Al(6), which may be more valid for the Li-richer micas but is not valid for most biotites. The latter, in our granites, contain relatively small, but significant amounts of Mg (and also some Mn), and whilst Li_2O–MgO correlation is lower than that of Li_2O–FeO (Table 3); it is, nevertheless, significant. If we rewrite the equation as

$$K_2R_x^{2+}Li_{4-x}R_2^{3+}(Al_xSi_{8-x})(OH,F)_4$$

it is more applicable, although values of R^{2+} + Li in our data vary between 2.5 and 4.0 and R^{3+} varies from 1.8 to 2.6, generally increasing, as a result of higher Al(6), with increasing Li. In our samples, the value of Fe^{2+} + Li is close to 3 (Fig. 5*a*), that of R^{2+} + Li is nearer to 3.5 and, indeed, the whole octahedral site contains about 5.5 cations per formula unit.

The ranges in the Li–Fe micas proposed by Rieder and by Foster on the basis of Li atoms in the unit formula, together with a suggested compromise are as follows:

	Foster	Rieder	This paper
Siderophyllite	<0.5	<1.0	<1.0
Protolithionite	0.5–1.5	—	—
Zinnwaldite	1.5–2.5	1.0–3.0	1.0–2.5
Lepidolite	>2.5	>3.0	>2.5

The newly proposed ranges provide only a guide as Li + R^{2+} is rarely equal to 4, but they can be related more closely with the simpler and more readily understandable Foster diagram. By eliminating protolithionite from this series, as proposed by Rieder, the zinnwaldite boundary is extended downwards and that of siderophyllite upwards to about 1.0 Li atoms. The old range of protolithionite is now occupied by the lithian siderophyllites and the ferroan zinnwaldites. On the basis of Li + R^{2+} = 3.5 (a value close to that in most of these micas) the boundary between siderophyllite and zinnwaldite occurs at a Li:R^{2+} ratio of 1:2.5, close to the line at $Li_{30}R_{70}^{2+}$ in Fig. 3. Likewise, the zinnwaldite–lepidolite boundary at Li = 2.5 gives Li:R^{2+} = 2.5:1, close to $Li_{70}R_{30}^{2+}$ in Fig. 3. These ratios can be used for classification irrespective of the total value of Li + R^{2+}, provided that the total octahedral ions lie between 5 and 6 (i.e. the mica is trioctahedral). However, owing to the multivariate nature of the data, no clear-cut boundary lines between these micas can be expected and zones of transition will occur. The composition ranges in terms of Li and R^{2+} proposed here apply to the data of Table 4 and to the data of Foster and will be generally applicable when the octahedral cation sum <6 and Li + R^{2+} < 4 in most cases.

The 'biotites' in Table 4 (cols. 1–11) have ranges in the octahedral cations as follows: Al = 1.031 – 1.756; R^{3+} (including Ti^{4+}) = 1.720–2.026; Li = 0.304–0.982. With the exception of two samples from the St. Austell pluton (Table 2, cols. 1 and 3), they straddle the protolithionite–siderophyllite boundary of Foster (1960) in the octahedral Li–R^{3+}–R^{2+} diagram (Fig. 3) and while their Li contents place them amongst the Li-rich siderophyllites, their relatively low Fe contents put them close to her 'protolithionites'. In the Rieder (1970) diagram, on the other hand, these micas plot well away from the ideal composition of protolithionite which, like zinnwaldite, lies on the annite–trilithionite sideline, but closer to annite (Fig. 4). The Cornubian 'biotites', having tetrahedral Al = 2.25–2.82 (fig. 5*c*) and octahedral Fe^{2+} = 2.09–2.76, lie well below the range of x proposed for siderophyllite by Rieder (1970), but the Li values of 0.30–0.99 (or 0.60 if the St. Austell examples are excluded) are below the range of x required for zinnwaldite.

Tetrahedral Al contents plotted against $Fe^{2+}/(Fe^{2+} + Mg)$ suggest compositions between annite and siderophyllite (Fig. 5*c*), but the octahedral Al contents place these 'biotites' close to siderophyllite (Fig. 5*d*). The trend towards annite in Fig. 5*c* and the increased octahedral Al at high $Fe^{2+}/(Fe^{2+} + Mg)$ ratios reflect the trend of these biotite compositions towards zinnwaldite along the X–Y line in Fig. 4. Two zinnwaldite data points that fall in the field covered by Fig. 5*d* are plotted in order to illustrate this biotite trend.

On the basis of the proposed classification, all the Cornubian 'biotites' are siderophyllites, and most (with >0.5 Li in the formula) are best regarded as lithian siderophyllites with low Fe^{2+}, R^{3+} and commonly K, compensated by excess Si.

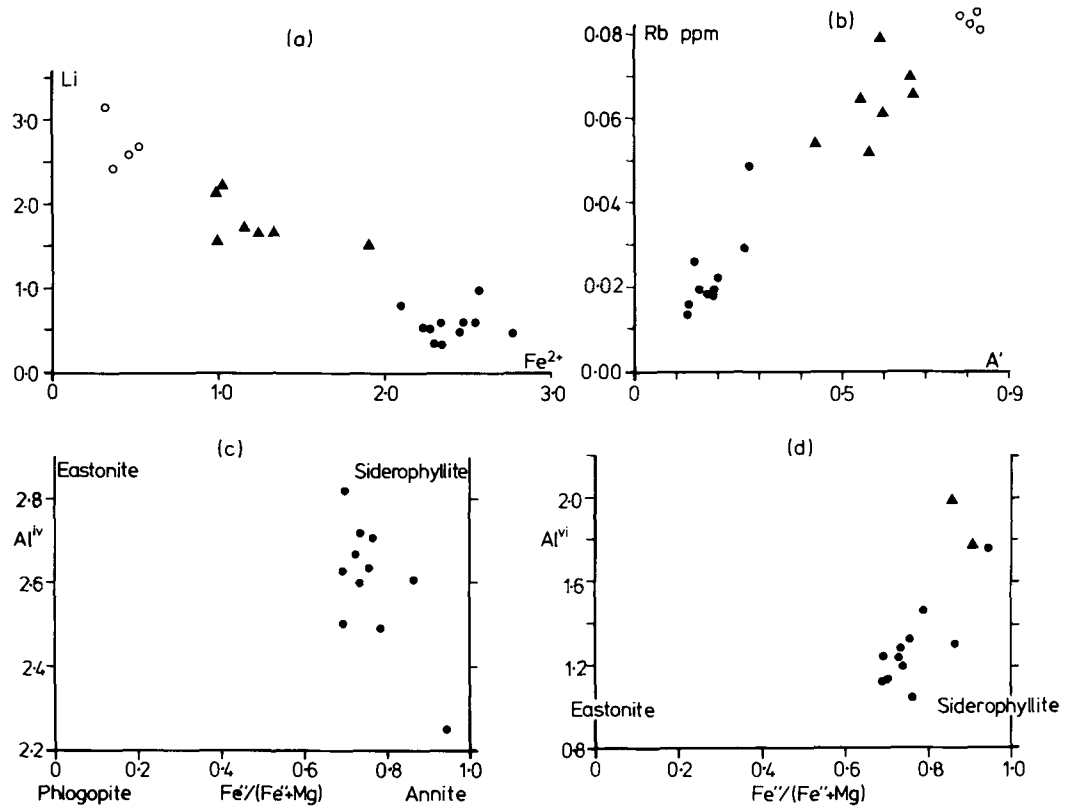

FIG. 5. Formula variation diagrams: (*a*) Li–Fe^{2+}; (*b*) Rb–*A'*, where $A' = LR/(LR + \text{"Fe"})$; (*c*) tetrahedral Al *vs.* $Fe^{2+}/(Fe^{2+} + Mg)$; (*d*) octahedral Al *vs.* $Fe^{2+}/(Fe^{2+} + Mg)$. Symbols as in Fig. 2.

Specimen E259 (Table 2, col. 3) is the so-called zinnwaldite from the Trelavour Downs pegmatite, but despite its high Li and F contents is actually a lithian siderophyllite. Low K is likely to reflect substitution by H_3O^+.

Charoy (1986) has not included Li in his structural formula and has calculated the Fe content of Carnmenellis micas from the bulk rock composition so that his findings are not directly comparable with ours. So far as Al, Fe and Mg are concerned, the results are broadly similar.

The 'zinnwaldites' (Table 4, cols. 12–18) of this paper fall clearly into the field of zinnwaldites, as indicated both by Rieder (1970) and by Foster (1960). All their Li contents fall within the range of 1 and 2.5 proposed herein for zinnwaldites and their Li : R^{2+} ratios lie between 3 : 7 and 7 : 3.

The 'lepidolites' (Table 4, cols. 19–22) of this paper have $x < 1$ for both tetrahedral Al and octahedral Fe^{2+} and have Si > 7, but are low in Li: only one (no. 21) has Li > 3. They can be considered as ferroan lepidolites falling on the field boundary between zinnwaldite and ferroan lepidolite of Rieder (1970), although on the basis of their Li content in the classification of Foster (1960) and the ranges proposed here, they are true lepidolites (no. 20 with 2.43 Li is just below the lower limit of 2.5). By contrast, lepidolites from the Meldon microgranite dyke, north-west of Dartmoor have octahedral $Fe^{2+} < 1$, but tetrahedral Al > 1 and Si < 7 (Chaudhry and Howie, 1973*a*, Table I). Most of these have Li greater than or close to 3.

Microanalytical data

Results obtained by microprobe analysis exclude Li; where this element is significant in amount, as in the Cornubian micas, analyses are incomplete and realistic formulae cannot be calculated. Some Li data for micas from the Cornubian batholith have been obtained using an ion probe by Wilson and Long (1983) and by Martin (1983,

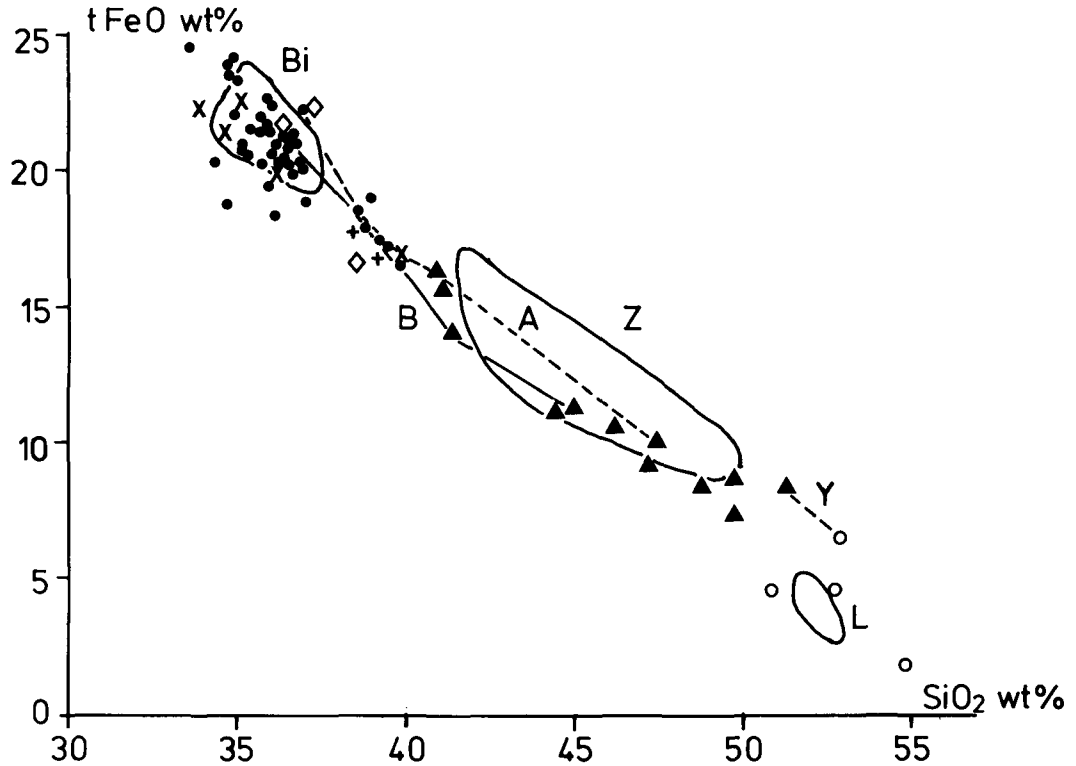

FIG. 6. Total Fe as FeO *vs.* SiO_2 (wt. %) plot for all data: distribution of the 22 XRF analyses marked by fields Bi (biotite), Z (zinnwaldite) and L (lepidolite). Symbols for earlier biotite analyses as in Fig. 3, except for Dartmoor biotites now shown as ◇: in addition, microprobe data points shown as • for biotite, ▲ for zinnwaldite and ○ for lepidolite. A and B show the trends of biotite to zinnwaldite transformation in the two traverses in hornfels at Type G granite contact (Table 5): Y gives composition points showing change from zinnwaldite to lepidolite in pegmatite from Roof Complex of Tregonning granite.

1984). Plots of microprobe data give similar patterns and groupings to those of the 22 XRF and wet analyses considered in the previous sections of this paper. An example is shown in the tFeO–SiO_2 plot shown in Fig. 6. In general, the probe data tend to increase the overall data spread, thereby enhancing the continuity between the lepidolites and biotites. The zinnwaldite and biotite 'fields' are completely bridged by the data of Table 5 plotted as trends A and B in Figs. 6 and 7, while the zinnwaldite and lepidolite 'fields' are largely closed by data points for a pegmatite specimen (Y in Fig. 6). All these data convincingly demonstrate the continuity between siderophyllite and lepidolite within the Li–Fe micas.

Classification of these micas is best obtained from their formulae but, where these cannot be calculated with confidence, the weight percentages of oxides provide a guide. As rough indications, zinnwaldites having between 1 and 2.5 Li atoms per formula unit contain about 1.8–4.5 wt. % Li_2O and <20.0–8.0 wt. % FeO; siderophyllites have <1.8 wt. % Li_2O and >16.0 (usually >20) wt. % FeO; and lepidolites have >4.5 wt. % Li_2O and <8.0 wt. % FeO. These are only rough figures, based upon those given by Foster (1960): obviously, marked variation in other oxides, particularly Al_2O_3, Fe_2O_3 and SiO_2, which have significantly different 'molecular weights' from Li_2O and FeO, can affect the percentages of the latter.

Thus, microprobe data for tFeO provide a rough guide to the position of a mica within the Li–Fe mica series. Under the microscope, lepidolite is not readily distinguished from muscovite, but Al_2O_3 obtained by microprobe analysis provides a simple means of distinguishing between these minerals. The wt. % Al_2O_3 in lepidolite is generally close to about 20% (19–22%, extending to 26% in the Meldon data) and is typically 30%

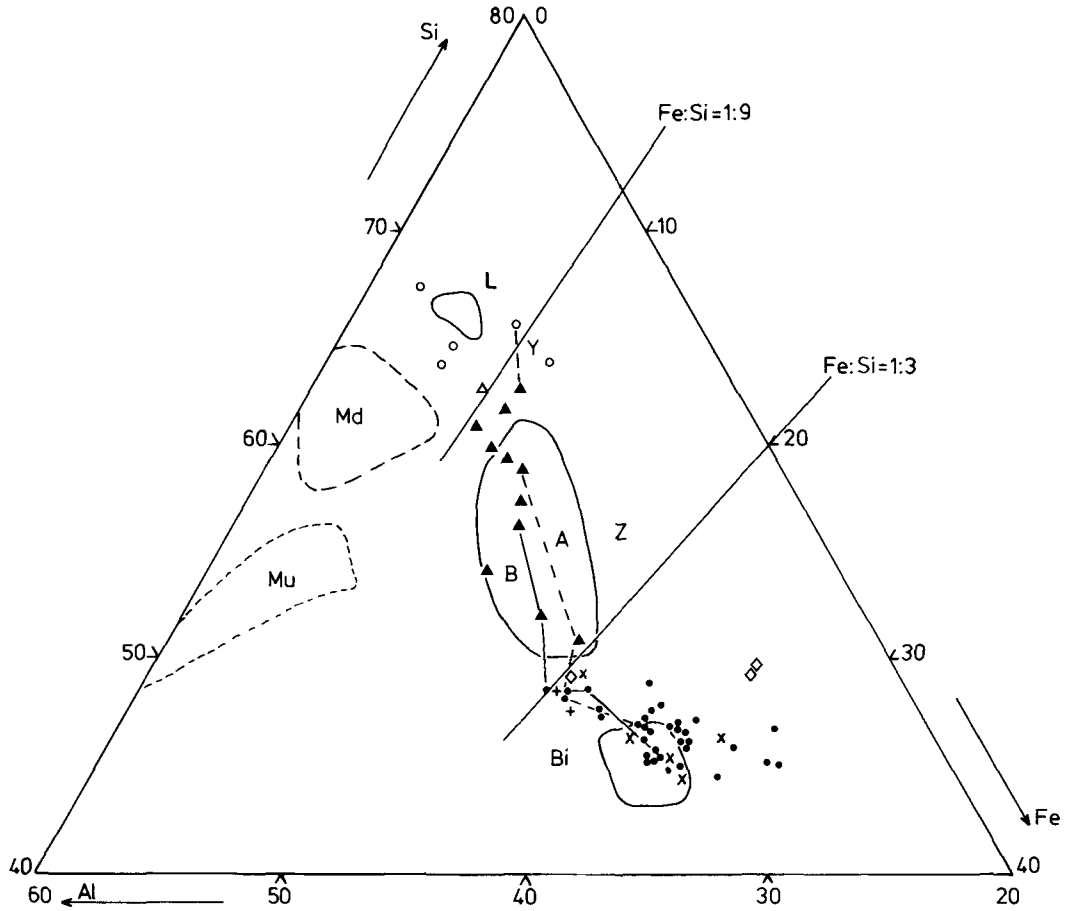

FIG. 7. Plot of atomic percentages of Si, Al and total iron as Fe^{2+}. Microprobe symbols as in Fig. 6, biotite symbols (non-microprobe) as in Fig. 3. △ = zinnwaldite (Cundy *et al.*, 1960). Fields Bi, Z and L and trends A, B and Y as in Fig. 6. Md—field of Meldon lepidolites; Mu—field of muscovites from the Cornubian batholith [this includes data from Meldon (Chaudhry and Howie, 1973*b*), Cligga (Hall, 1971) and 30 data points obtained by electron microprobe analysis (Stone, unpublished)]. Also shown are the approximate boundaries between lepidolite and zinnwaldite (at Fe : Si = 1 : 9) and between zinnwaldite and siderophyllite (at Fe : Si = 1 : 3).

or more in muscovite. A more comprehensive discrimination between all these micas is obtained using a triangular plot of atomic percentages of Fe, Al and Si (Fig. 7). This shows the fields outlined by the chemically analysed micas, the continuity between the fields of the Li–Fe micas, and the separation of the muscovite and lepidolite fields (although one Meldon lepidolite lies close to the muscovite field). Additional significant differences between lepidolite and muscovite include the higher Rb_2O and F of the former (near 1% and generally over 6% respectively) compared with the latter (below 0.5% and 3% respectively for the few analysed from the Cornubian batholith). The field boundaries between siderophyllite and zinnwaldite on the one hand and zinnwaldite and lepidolite on the other lie at Fe : Si ratios of about 1 : 9 and 1 : 3 respectively. Further work on the white micas is currently in progress.

Some biotites analysed by microprobe showed small decreases in TiO_2, tFeO and MnO and increases in MgO, Rb_2O and F from centre to edge of grains, but errors introduced by taking average values of these slightly zoned biotites are likely to be small and direct comparison can confidently be made with bulk biotite analyses. Zinnwaldite and lepidolite may show more marked zoning, as indicated below, and comparisons

Table 6. Average compositions of lithium iron micas in different rock types

	1	2		3	4		5		6	
Type	A	B		'C'	HFS		E		G	
	Biotite						Zinnwaldite		Lepidolite	
	wt%	wt%	s	wt%	wt%	s	wt%	s	wt%	s
SiO_2	35.07	35.80	1.03	37.42*	36.03	1.22	47.06	2.96	52.35	1.35
TiO_2	3.29	2.57	0.56	1.94	2.29	0.31	0.48	0.39	0.19	0.05
Al_2O_3	18.55	21.10	1.17	22.53	19.73	2.13	21.70	1.33	20.43	0.88
tFeO	22.84	21.40	1.25	20.78*	19.65	1.21	10.74	2.60	3.67	1.11
MnO	0.45	0.40	0.13	0.52	0.31	0.13	0.47	0.14	1.15	0.12
MgO	5.09	4.13	1.15	1.90*	7.01	3.07	0.36	0.38	0.12	0.13
Na_2O	0.15	0.25	0.30	0.16*	0.19	0.11	0.61	0.61	0.23	0.19
K_2O	9.33	8.91	0.51	9.53	9.18	0.36	9.44	0.26	9.27	0.19
Rb_2O	0.16	0.23	0.08	0.34	0.21	0.16	0.72	0.10	0.96	0.04
Cs_2O	0.02	0.05	0.03	0.11	0.06	0.04	0.13	0.07	0.14	0.04
SnO	0.01	0.02	0.03	0.00	0.01	0.03	0.01	0.01	0.01	--
F	1.70	2.00	0.75	2.78	1.80	1.42	5.98	1.12	7.55	0.59
n =	4	25		2	8		10		6	

* wide differences between the two analyses.
s = one standard deviation where number of samples, n > 5
'C' = biotite microgranites; HFS = hornfelses: other rock types as already indicated in Table 1.
tFeO is total iron as FeO.

between probe and bulk analyses require more caution, although similar overall differentiation trends are revealed quite clearly both by probe- and bulk-analysed micas. However, for the purposes of nomenclature, ranges in composition zoning, when present, should be stated and bulk analysis should be clearly indicated in the case of mineral separates.

Distribution and origin of the Li–Fe micas

The average compositions of trioctahedral micas from the Cornubian batholith that have been analysed for Rb, Cs and F in addition to the usual major elements in each of 6 types of host rock are given in Table 6. The basic data include the 22 fully analysed samples (Table 2) and the mica averages in 33 samples determined with the CAMECA microprobe at Manchester.

The order of development of the granite host rocks of the analysed micas is A–B(–C)–E–G (Exley and Stone, 1982). Type A occurs as inclusions in Type B, whilst C occurs as dykes that cut Type B. Type E is intrusive into Type B in the St. Austell pluton and veins of this type cut the Type C (Godolphin) granite in the Tregonning–Godolphin pluton. Type G occurs as a roof differentiate of E. The evolution of micas in the B–E–G sequence is obvious in Table 6. The significant increases in MnO, Rb_2O, Cs_2O and F are reflected also in the host rocks (Stone, 1975; Exley and Stone, 1982) as also are the marked decreases in TiO_2, tFeO and MgO. The increase in SiO_2, on the other hand, is not apparent in the host rocks.

Biotite. Differences between the biotites of cols. 1, 2 and 4 of Table 6 were examined by one way analysis of variance. Significant values of the F statistic at the 0.05 probability level lead to the rejection of the Null hypothesis that all these groups come from the same population for TiO_2, Al_2O_3, tFeO and MgO. This is confirmed even more forcibly using the equivalent non-parametric Kruskall–Wallis test, with the rejection of H_0 in each case at the 0.01 probability level. The Minitab printout of the 95% confidence intervals about the mean for each rock type indicates those rock types responsible for the significant differences: Type A granite inclusions (col. 1) have higher TiO_2 and tFeO than the other two types, the Type B granite biotites (col. 2) are richer in Al_2O_3 and hornfels biotites have higher MgO (the hornfelses themselves have much higher MgO contents than the granites). The two microgranite

biotites (col. 3, not tested owing to small sample size) tend to be lower in femics and higher in Rb and Cs and, perhaps, F, than their host rocks, consistent with a proposed origin as late differentiates of Type B granite magmas.

Textural studies suggest that biotite crystallized early or is a restite phase that subsequently equilibrated in the magmatic and, perhaps, post-magmatic environment (Stone, 1979; Charoy, 1986). The small, though sometimes significant, differences between the three types of biotite are attributed to progressive differentiation of the host rocks, perhaps initially from a Type A granite magma. Charoy (1986) has suggested that the Carnmenellis Type B granite magma is derived from pelitic sedimentary rocks of Brioverian age. The present MgO-poor mica compositions of the granites do not reflect this, although original Mg-richer biotites, like those in the hornfelses, would be expected to undergo re-equilibration involving increasing $Fe^{2+}/(Fe^{2+} + Mg)$ with evolving magma generated initially by the partial fusion of pelitic rocks.

Zinnwaldite. Analyses of micas from the Type E granites and one from a Type D granite are given in cols. 14–18 of Tables 2 and 4. The mica from the Type D granite (col. 12) is richer in TiO_2, Fe_2O_3 and MgO and poorer in SiO_2 compared with most of the Type E granite zinnwaldites. The latter type from St. Austell (col. 13) compares quite closely with the Tregonning zinnwaldites. Amongst the latter, specimen 0002 (col. 14) is enriched in TiO_2, FeO, MgO and Cr, V and Zr, and comes from a contact facies. It is currently believed that both Types E and B granites are magmatic and that the former has been derived from the latter by magmatic differentiation (Manning, 1982) or by metasomatism (Stone, 1975, 1984). Late differentiates in the Carnmenellis Type B granite complex do have some features that could relate them to a magmatic trend whose end products were Li-mica granites (Charoy, 1986) and the experimental work of Manning (1981) shows that, in the alkali feldspar granite system, high fluorine contents move a ternary minimum/eutectic towards the albite corner of the Qz–Ab–Or triangle and result in the simultaneous precipitation of two alkali feldspars along with quartz, consistent with textural evidence from the Type E granites (Stone, 1984). However, there is little field evidence for the direct magmatic evolution from type B to Type E granites. Most of the plutons in the batholith have no Li-mica granites associated directly with them and the isolated mini-pluton of Porthmeor exhibits a differentiated roof zone showing some enrichment in Li, Rb, Cs and F, but without the development of Type E granite. On the other hand, Dangerfield *et al.* (1980) have shown that biotite granites intruded by Type E granite at St. Austell have a marked Li enrichment aureole. This aureole is composed of Type D granite (Exley and Stone, 1982), which, on the basis of major elements, clusters with the Type B granites (Stone and Exley, 1978), but has many mineralogical and chemical features that are transitional between Types B and E. In addition, the data presented in Table 5 show that there is a complete series between siderophyllite and zinnwaldite and that the latter can be derived from the other by metasomatic ion exchange. Taken together, these features are considered as evidence for a metasomatic origin of the Type D granites (Manning and Exley, 1984).

This type of evidence led Stone (1984) to suggest that the exchange of Mg and Fe by Li in the micas together with the removal of Ca from plagioclase feldspar and metasomatic Na enrichment could lead to remobilization and the production of Type E granite magma below the present erosion surface. It is considered that no large thermal energy input would be needed for the relatively small amounts of magma required to account for the present distribution of Type E granites. On the other hand, there is clear textural evidence for the replacement of K-feldspar by zinnwaldite, implying late-stage growth (Stone, 1984), perhaps upon earlier-formed interstitial grains.

Martin (1983) considers that interstitial Li–Fe micas in the Type E granite of the St. Austell pluton are primary, whereas those micas in the Type D granite may have a different origin. Microprobe/ion probe analyses of Li-Fe micas from the Types D and E granites of St. Austell by this author reveal mainly zinnwaldites in Type D and compositions on or close to the zinnwaldite–lepidolite boundary in Type E (some have Li > 3 in the formula but an Li/R^{2+} ratio close to 0.70). However, fluctuations in composition points that contribute to average specimen analyses commonly cross this boundary. This is clearly the case in some examples of zoning in which the Li_2O content increases and that of tFeO decreases from centre to edge of a grain. Recent work by Henderson, Martin and Mason (C.M.B. Henderson, pers. comm.) confirms these zoning trends and shows substantial zoning ranges in D and E type granites. However, micas from the most evolved E-type granites lie completely within the lepidolite field.

Lepidolite. Textural evidence (Stone, 1984) points to the late growth of lepidolite in some pegmatites at the Megiliggar Rocks, although those of the lepidolite–albite–topaz leucogranites (Type G) in the roof zone overlying the Type E

Tregonning granite appear to be primary and to have crystallized from magma simultaneously with quartz and two alkali feldspars (Stone, 1984).

The lepidolites of the Meldon microgranite have generally higher Li, Rb and Cs and lower Fe^{2+} and Mn than the leucogranite lepidolites in the Tregonning–Godolphin pluton (Tables 2 and 4, cols. 19–22). The latter lepidolites are 1*M* polytypes, similar to the 1*M* lepidolites of the Meldon microgranite in having higher FeO and MnO contents, and consequently lower A′ values than the Meldon $2M_2$ lepidolites. The latter come from pegmatites in the Meldon microgranite and are considered by Chaudhry and Howie (1973*a*) to have crystallized in a volatile-rich, relatively low-temperature environment compared with the 1*M* polytypes that are believed to have formed in higher temperature, volatile-poor environments. This accords with textural evidence, which suggests that the 1*M* lepidolites from the Tregonning leucogranites belong to a primary magmatic stage (Stone, 1984).

Acknowledgements

The authors would like to thank Messrs Tim Hopkins and Dave Plant of the Department of Geology, University of Manchester, for their unstinting help to M.S. in the use of the C.A.M.E.C.A. electron microprobe and to Mr John Merefield for the chemical analyses of micas at the University of Exeter. Thanks are also due to Dr C. M. B. Henderson for his critical reading of the manuscript and helpful suggestions. Grants from the Research Funds of the Universities of Exeter and Keele to M.S. and C.S.E. respectively, for the initial field work, are gratefully acknowledged.

References

Al-Saleh, S., Fuge, R. and Rea, W. J. (1977) *Proc. Ussher Soc.* **4**, 37–48.

Barrière, M. and Cotten, J. (1979) *Contrib. Mineral. Petrol.* **70**, 183–92.

Charoy, B. (1986) *J. Petrol.* **27**, 571–604.

Chaudhry, M. N. and Howie, R. A. (1973*a*) *Mineral. Mag.* **39**, 289–96.

————(1973*b*) *Proc. Ussher Soc.* **2**, 480–1.

Cundy, E. K., Windle, W. and Warren, I. H. (1960) *Clay Minerals Bull.* **4**, 151–6.

Dangerfield, J., Hawkes, J. R. and Hunt, E. C. (1980) *Proc. Ussher Soc.* **5**, 76–80.

Deer, W. A. (1937) *Mineral. Mag.* **24**, 495–502.

Dodge, F. C. W., Smith, V. C. and Mays, R. E. (1969) *J. Petrol.* **10**, 250–7.

Exley, C. S. (1959) *Q.J. Geol. Soc.* **114**, 197–230.

——and Stone, M. (1964) *R. Geol. Soc. Cornwall*, 150th Anniv. Vol., 131–84.

————(1982) Hercynian intrusive rocks. In *Igneous rocks of the British Isles* (Sutherland, D. S., ed.) Wiley, Chichester, 287–320.

French, W. J. and Adams, S. J. (1972) *Analyst*, **97**, 828–31.

Foster, M. D. (1960) *U.S. Geol. Surv. Prof. Paper* 354-E.

Hall, A (1971) *Proc. Geol. Assoc.* **82**, 209–30.

Harvey, P. K., Taylor, D. M., Hendry, R. D. and Bancroft, F. (1973) *X-Ray Spectrometry*, **2**, 33–44.

Haslam, H. W. (1968) *J. Petrol.* **9**, 84–104.

Hawkes, J. R. and Dangerfield, J. (1978) *Proc. Ussher Soc.* **4**, 158–71.

Jefferies, N. L. (1984) Ibid. **6**, 35–41.

——(1985) *Mineral. Mag.* **49**, 495–504.

Joyce, A. S. (1973) *Chem. Geol.* **11**, 271–96.

Manning, D. A. C. (1981) *Contrib. Mineral. Petrol.* **76**, 205–15.

——(1982) In *Metallization associated with acid magmatism* (Evans, A. M., ed.) Wiley, Chichester, 191–203.

——and Exley, C. S. (1984) *J. Geol. Soc.* **141**, 581–91.

Martin, J. S. (1983) *An experimental and field study of late-stage Li-rich gfranites.* Unpubl. Ph.D. Thesis, Univ. of Manchester.

——(1984) *Proc. Ussher Soc.* **6**, 142.

Neiva, A. M. R. (1976) *Mineral. Mag.* **40**, 453–66.

Nockolds, S. R. and Mitchell, R. L. (1948) *Trans. R. Soc. Edinb.* **61**, 533–75.

Norrish, K. and Hutton, J. T. (1964) C.S.I.R.O. Div. Soils, Adelaide, S.A., Rept. 3/64, 10pp.

Palchen, W. and Tischendorf, G. (1974) In *Metallization Associated with Acid Magmatism*, Vol. 1 (Štemprok, M., ed.) Geol. Surv. Prague, 206–9.

Plimer, I. R. and Kleeman, J. D. (1986) *Trans. Inst. Min. Metall. (Sect. B, Appl. Earth Sci.)* **95**, B1–5.

Rieder, M. (1970) *Contrib. Mineral. Petrol.* **27**, 131–58.

Smith, T. E., Miller, P. M. and Huang, C. H. (1982) In *Metallization Associated with Acid Magmatism*, Vol. 6 (Evans, A. M., ed.), Wiley, Chichester, 301–20.

Štemprok, M. and Šulcek, Z. (1969) *Econ. Geol.* **64**, 392–404.

Stone, M. (1975) *Proc. Geol. Assoc.* **86**, 155–70.

——(1979) *Proc. Ussher Soc.* **4**, 370–9.

——(1982) In *Metallization Associated with Acid Magmatism*, Vol. 6 (Evans, A. M., ed.), Wiley, Chichester, 339–55.

——(1984) *Proc. Geol. Assoc.* **95**, 28–41.

——and Exley, C. S. (1978) *Proc. Ussher Soc.* **4**, 172–81.

Troll, G., Farzaneh, A. and Cammann, K. (1977) *Chem. Geol.* **20**, 295–305.

Wilson, G. C. and Long, J. V. P. (1983) *Mineral. Mag.* **47**, 191–9.

Appendix

Localities of analysed specimens in Tables 2 and 4

1. E179 (B). West side of railway cutting, 280 m south of Treffry viaduct, Luxulyan, St. Austell. GR: 056570.
2. EB5/2 (B). Gold-diggings Quarry, Bodmin Moor: 1700 m north-west of chapel at Minions (called 'Cheesewring Railway' on 1:25000 maps). GR: 249724.
3. E259 (B). Pegmatite, Trelavour Downs, St. Austell. GR: 960575.
4. MS0020 (B). Bosahan Quarry, Carnmenellis granite. GR: 729302.
5. MS0021 (B). Trolvis Quarry, Carnmenellis granite. GR: 743349.
6. MS0359 (B). Biotite pegmatite, Porthledden, Land's End granite. GR: 355321.
7. MS0465 (B). New Quay, St. Martins, Isles of Scilly granite. GR: 931151.
8. MS0467 (B'). Fine-grained biotite granite inclusion in Type B granite, Bryher, Isles of Scilly granite. GR: 877161.
9. MS0620 (B). Pelastine Quarry, Carnmenellis granite. GR: 735317.
10. MS0630 (B). Rosemanowas Quarry, Carnmenellis granite. GR: 735346.
11. MS0631 (B). Goodagrane Quarry, Carnmenellis granite. GR: 749330.
12. E249 (D). Gunheath China-clay pit (c. 200 m north-east of offices), St. Austell granite. GR: 002567.
13. E250 (E). Rostowrack Quarry, St. Austell granite. GR: 953566.
14. MS0002 (E). Tourmaline-rich granite near roof contact, Trewavas Head, Tregonning granite. GR: 592265.
15. MS0004 (E). Rinsey West Cliff, Tregonning granite. GR: 587273.
16. MS0007 (E). Small quarry, north north west of Lower Trevurvas, Tregonning granite. GR: 586287.
17. MS0045 (E). Trewavas Head, Tregonning granite. GR: 595265.
18. MS0088 (E). Eastern end of Praa Sands (Lesceave Por), Tregonning granite. GR: 586275.
19. MS0034 (G). Carn Clodgy, roof zone of Tregonning granite. GR: 695267.
20. MS0042 (G). Sheeted complex, Megiliggar Rocks. GR: 608267.
21. MS0083 (G). Roof zone of Tregonning granite, Trewavas Head. GR: 594266.
22. MS0084 (G). Sheeted complex, Megiliggar Rocks. GR: 607267.

[*Manuscript received 29 January 1987: revised 11 May 1987*]